Applied Catalysis B: Environmental 123–124 (2012) 351–356

Contents lists available at SciVerse ScienceDirect

Applied Catalysis B: Environmental

journal homepage: www.elsevier.com/locate/apcatb

# Quantitative analysis of active oxygen for soot oxidation over $Ag/ZrO_2$: Characterization with temperature-programmed reduction by $NH_3$

Tetsuya Nanba[a,*], Shoichi Masukawa[a], Akira Abe[b], Junko Uchisawa[a], Akira Obuchi[a]

[a] National Institute of Advanced Industrial Science and Technology (AIST), Research Center for New Fuels and Vehicle Technology, 16-1 Onogawa, Tsukuba 305-8569, Japan
[b] Mitsui Mining & Smelting Co., Ltd., 1013-1 Ageoshimo, Ageo 362-0025, Japan

ARTICLE INFO

*Article history:*
Received 30 October 2011
Received in revised form 26 March 2012
Accepted 1 May 2012
Available online 9 May 2012

*Keywords:*
Soot
Oxidation
Ag
$ZrO_2$
$H_2$-TPR
$NH_3$-TPR

ABSTRACT

Active oxygen species for soot oxidation over $Ag/ZrO_2$ were characterized by means of X-ray photoelectron spectroscopy (XPS) and temperature-programmed desorption and reduction methods. The temperature-programmed surface reaction (TPSR) between carbon black (CB), a model soot, and surface oxygen revealed that two kinds of adsorbed oxygen species were involved in CB oxidation over $Ag/ZrO_2$. The results of XPS, temperature-programmed desorption of $O_2$, and temperature-programmed reduction by $H_2$ were insufficient to distinguish the two kinds of active oxygen species. Temperature-programmed reduction by $NH_3$ ($NH_3$-TPR) resulted in $N_2$ and $N_2O$ formation as products of reduction of the $Ag/ZrO_2$ surface and bulk oxygen. The $N_2O$ formation profile in $NH_3$-TPR exhibited two peaks, corresponding to two kinds of oxygen species having a strong oxidation capacity. The effect of Ag loading on the total amount of $N_2O$ formation was in good agreement with that on the amount of active oxygen species observed by TPSR-CB. We concluded that $NH_3$-TPR was an appropriate technique for quantitative characterization of the amount of active oxygen species for soot oxidation on $Ag/ZrO_2$.



## 1. Introduction

Development of abatement technologies for particulate matter (PM) emitted from diesel engines is important for protecting human health. PM is mainly composed of solid carbonaceous compounds, soot, and soluble organic compounds, in which carcinogenic polycyclic aromatic hydrocarbons are contained [1]. Diesel particulate filter (DPF) systems are an effective and practical means for removing PM from diesel engine exhaust; however, DPF pores often become clogged by the accumulation of soot. Typically, DPFs are regenerated by intermittent heating to 600 °C to burn off the accumulated soot, but this regeneration process requires additional fuel consumption. To reduce fuel consumption, continuous regeneration of DPFs with the aid of a PM oxidation catalyst would be desirable.

Researchers at Johnson Matthey have developed the continuously regenerating trap (CRT) system, which works in the diesel exhaust temperature range of 180–300 °C [2]. The system contains an oxidation catalyst, such as Pt, placed in front of a DPF. NO in the exhaust gas is oxidized to $NO_2$ on the Pt catalyst, and this $NO_2$ oxidizes soot trapped on the DPF. In this process, the Pt catalyst oxidizes soot indirectly, using $NO_2$ as a mediator.

Another type of catalyst, which is supported on a DPF and directly promotes PM oxidation, has been frequently studied. Among the candidates of this type of catalyst are $CeO_2$ [3,4], mixed oxides of $CeO_2$ and metal oxides [5–8], and perovskites [9,10]. These oxides can catalyze the oxidation of soot with oxygen, and the presence of NOx can increase the extent of soot oxidation by indirect oxidation as well as Pt catalyst [11]. Many researchers have attempted to identify the active oxygen species responsible for soot oxidation on these catalysts and the soot oxidation reaction mechanism. For $CeO_2$ and other oxides having oxygen storage capacity, there are two kinds of proposed mechanisms: (i) the oxygen released from the oxide lattice oxidizes soot [12,13] and (ii) soot is oxidized by peroxide and/or superoxide formed at surface vacant oxygen sites, which are formed by release of oxygen from these oxygen storage materials [4,14]. These reaction mechanisms are under discussion.

Additional loading of metal components on these materials is effective for further decreasing the PM oxidation temperature [15,16]. Among these components, $Ag/CeO_2$ is known to be a very active catalyst. Shimizu et al. [17] proposed that active oxygen is formed at vacant oxygen sites on the $CeO_2$ surface and that Ag promotes the formation of these vacant sites in a manner similar to mechanism (ii) described above. Aneggi et al. [18] reported that the activity of $Ag/ZrO_2$ is comparable to that of $Ag/CeO_2$. Although $ZrO_2$ has a capacity for oxygen ion conductivity, the migration of oxygen does not occur easily at 300 °C, the temperature at which $Ag/ZrO_2$ shows soot oxidation activity [19]. The fact that $Ag/ZrO_2$

* Corresponding author. Tel.: +81 29 861 8717; fax: +81 29 861 8259.
*E-mail address:* tty-namba@aist.go.jp (T. Nanba).

0926-3373/$ – see front matter © 2012 Elsevier B.V. All rights reserved.
http://dx.doi.org/10.1016/j.apcatb.2012.05.001

shows high soot oxidation activity means that Ag not only promotes the migration of oxygen in support materials but also serves as an active site for soot oxidation. In fact, Ag itself is known to be an active component for soot oxidation, as it has high mobility to penetrate into and oxidize graphite [20]. We also previously reported that the number of Ag nanoparticles having a diameter of 2–10 nm on $ZrO_2$ is correlated with the observed rate of soot oxidation [21].

In this study, we aimed to characterize in greater detail the active oxygen species on Ag active sites of $Ag/ZrO_2$ catalysts for soot oxidation. We performed conventional thermal analyses, such as temperature-programmed reduction by $H_2$ and temperature-programmed desorption of $O_2$. Additionally, we have developed a novel method for temperature-programmed reduction by $NH_3$, which we found to be a powerful technique for quantitative analysis of the active oxygen species.

## 2. Experimental

### 2.1. Catalyst preparation

$Ag/ZrO_2$ was prepared by means of impregnation with $AgNO_3$ (Wako Pure Chemical Industries) and $ZrO_2$ (RCS-H; Daiichi Kigenso) as precursors. Various catalysts with a different Ag loading ranging from 0.5 to 20 wt% were prepared. After Ag loading, the samples were calcined at 500 °C for 4 h.

### 2.2. Activity measurements

Catalytic activity tests were carried out using a fixed-bed flow reactor system at atmospheric pressure. A commercial carbon black (CB: 7350F, Nippon Tokai Carbon) was used as a model soot. $Ag/ZrO_2$ and CB were mixed at a ratio of 100:1 with an agate mortar to form tight contact, and the mixture was pelletized and sieved to 0.15–0.25 mm. The temperature-programmed surface reaction of CB (TPSR-CB) and oxygen was carried out over $Ag/ZrO_2$. The mixture of $Ag/ZrO_2$ and CB described above was pretreated at 250 °C in He flow (50 ml/min) for 1 h to remove $CO_2$ weakly adsorbed on $ZrO_2$ and was cooled to room temperature. Then $O_2$ adsorption was carried out by introducing 10% $O_2$/He for 1 h, followed by He purge for 30 min. Under He flow, the temperature was raised at a rate of 10 °C/min, and $CO_2$ formation was monitored by a mass spectrometer (MS).

### 2.3. Catalyst characterization

Surface oxygen was analyzed by means of X-ray photoelectron spectroscopy (XPS; Shimazu, ESCA750).

Temperature-programmed desorption of $O_2$ ($O_2$-TPD) was carried out with the same flow reactor used for the catalytic activity test. As a pretreatment, the sample was heated at 500 °C for 1 h, cooled to 100 °C in 5% $O_2$/He, and then purged with He for 1 h. Under 100 ml/min of He flow the temperature was raised at a rate of 5 °C/min, and the $O_2$ concentration in the effluent was measured by a micro gas chromatograph (micro-GC; M200, Agilent) equipped with an MS-5A plot column and thermal conductivity detector.

Temperature-programmed reduction by $H_2$ ($H_2$-TPR) was carried out using the same flow reactor with a gas flow rate of 50 ml/min. The sample was pretreated at 500 °C for 1 h, cooled to 150 °C in 5% $O_2$/He, and the gas then switched to He. After the catalyst temperature reached room temperature or −70 °C under He, the temperature was raised at a rate of 10 °C/min in 2% $H_2$/He. The effluent gas was mixed with 2.4% $O_2$/He with a gas flow rate of 30 ml/min and then passed over a $Pt/Al_2O_3$ catalyst to react residual $H_2$ with $O_2$. $O_2$ concentration in the effluent from the $Pt/Al_2O_3$ reaction was measured by MS or by an $O_2$ analyzer, and an $H_2$ consumption profile was estimated from the change in $O_2$ concentration.

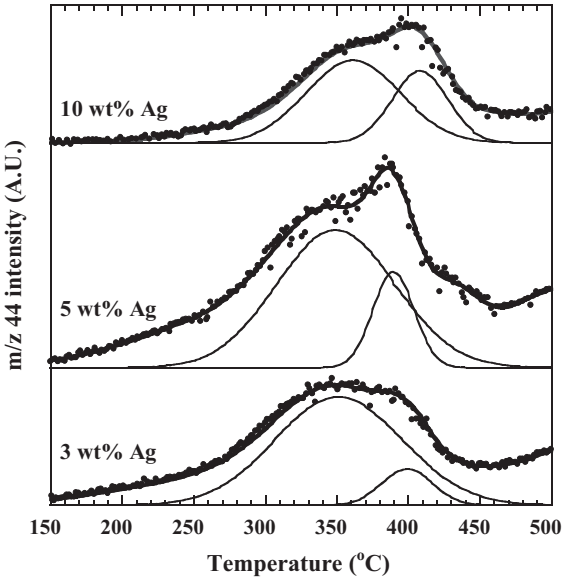


**Fig. 1.** $CO_2$ formation profiles (circles) and Gaussian fitted curves (solid lines) for 3, 5, and 10 wt% $Ag/ZrO_2$ during the temperature-programmed surface reaction of CB with preadsorbed oxygen. The weight of each mixture of catalyst and CB was 0.1 g. The flow rate was 50 ml/min. $O_2$ adsorption was carried out at room temperature after pretreatment at 250 °C in He.

Temperature-programmed reduction by $NH_3$ ($NH_3$-TPR) was carried out in the same flow reactor with a flow rate of 160 ml/min. The sample was pretreated at 500 °C for 1 h, cooled to 80 °C in 5% $O_2$/He, and the gas then switched to He. After the catalyst temperature reached room temperature under He, the temperature was raised at a rate of 5 °C/min in 0.1% $NH_3$/He. The effluent gas was analyzed by Fourier-transform infrared spectroscopy (Magna 560, Nicolet) with a multi-reflectance gas cell for $NH_3$ analysis, a micro-GC (M200, Agilent) equipped with an MS-5A and PoraPLOT Q column and thermal conductivity detectors for $N_2$ and $N_2O$, respectively, and another micro-GC (CP-2003, Variant) equipped with an MS-5A column and thermal conductivity detector for $H_2$ analysis.

## 3. Results and discussion

### 3.1. Catalytic activity for carbon black oxidation

We previously reported that CB oxidation activity increased with increasing Ag loading up to 5 wt% before decreasing with further increasing of Ag loading [21]. The maximum activity was obtained at 5 wt% Ag loading, and the next-most-active Ag loadings were 3 and 10 wt%.

We have also previously conducted TPSR-CB. From those results, we have determined that $CO_2$ formation below 460 °C should be due to the reaction between CB and preadsorbed $O_2$ on Ag particles [21]. Here, we attempted to deconvolute $CO_2$ formation by Gaussian fitting for 3–10 wt% Ag loading, and the results are shown in Fig. 1. Two peaks at 340–350 and 390–410 °C appeared, suggesting that two kinds of surface oxygen species reacted with CB on Ag particles. Here, we refer to the surface oxygen involved in CB oxidation as "active oxygen species." We attempted to characterize two kinds of active oxygen species.

### 3.2. XPS measurement for analysis of active oxygen species

To confirm that two kinds of oxygen species were involved in CB oxidation, XPS measurements were obtained. The O 1s XPS

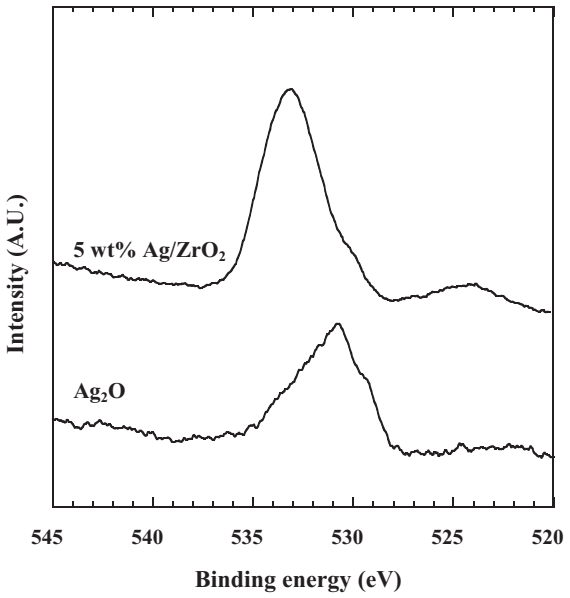


**Fig. 2.** XPS spectra of O 1s binding energy for wt% $Ag/ZrO_2$ and for $Ag_2O$.

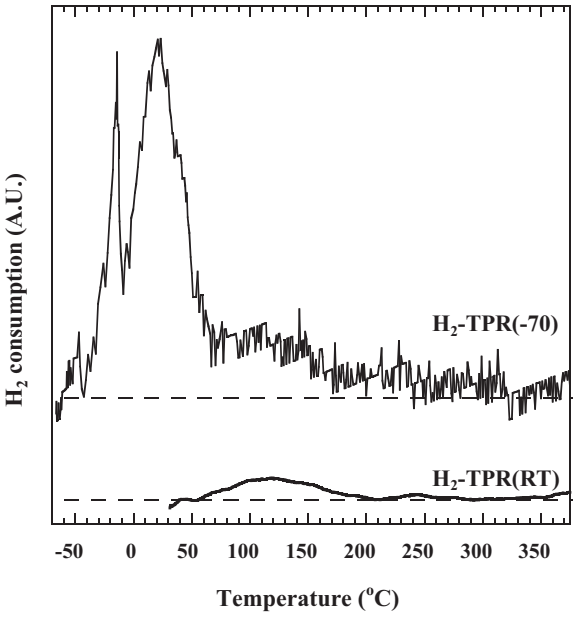


**Fig. 4.** $H_2$-TPR profiles from room temperature and −70 °C for 5 wt% $Ag/ZrO_2$.

profile for 5 wt% $Ag/ZrO_2$ is shown in Fig. 2. The O 1s binding energy was 533 eV, with an apparent shoulder at 530 eV. The 533 eV peak was assigned to surface oxygen species on $ZrO_2$ [22]. For reference, the XPS spectrum for $Ag_2O$ was also acquired (Fig. 2). The binding energy of O in $Ag_2O$ was 530.8 eV. Therefore, the shoulder at 530 eV in the $Ag/ZrO_2$ spectrum was assigned to O in $Ag_2O$. These results provide evidence of the presence of oxygen in $Ag_2O$. Two kinds of active oxygen species from the TPSR-CB were not distinguished by XPS.

### 3.3. $H_2$-TPR and $O_2$-TPD

We performed $O_2$-TPD for 5 wt% $Ag/ZrO_2$ (Fig. 3). $O_2$ desorption started at 220 °C, and only a single desorption peak centered at 325 °C was observed, indicating that the two kinds of active oxygen species suggested from the TPSR-CB results were not distinguishable with this method.

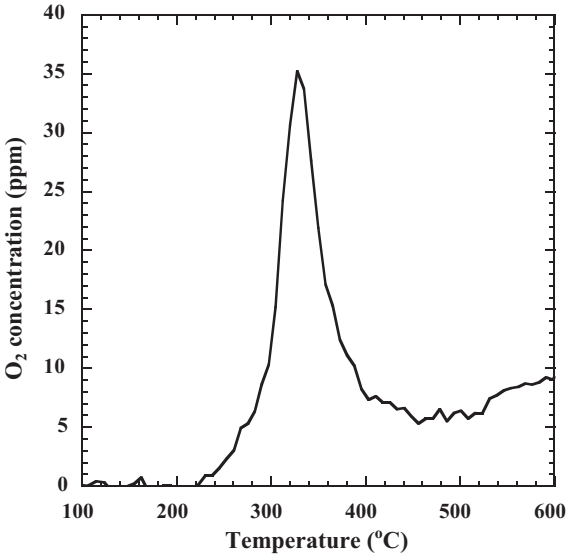


**Fig. 3.** $O_2$-TPD profile for 5 wt% $Ag/ZrO_2$.

Next, we performed $H_2$-TPR. Two $H_2$-TPR profiles for 5 wt% $Ag/ZrO_2$ are shown in Fig. 4. The $H_2$-TPR profile measured from room temperature ($H_2$-TPR(RT)) shows a broad and small $H_2$ consumption peak centered at 120 °C, with a corresponding $H_2$ consumption of 7 μmol/g. There is no indication of the presence of two kinds of oxygen species from this TPR profile.

We then performed $H_2$-TPR from −70 °C ($H_2$-TPR(−70)), and the resulting profile is also shown in Fig. 4. $H_2$ was consumed above −50 °C, and three peaks were observed at −15, 20, and 120 °C. The total $H_2$ consumption of these three peaks was 41 μmol/g. Compared with the $H_2$-TPR(RT) profile, the $H_2$ consumption markedly increased. Since $H_2$ is a strong reductant, oxygen species having high reactivity would react with $H_2$ even at room temperature, and we refer to such oxygen species here as "reactive oxygen species." The difference in $H_2$ consumption between $H_2$-TPR(RT) and $H_2$-TPR(−70) corresponds to the amount of reactive oxygen species that was present. In discussing the peak temperatures of these two TPR profiles, we pay special attention to the $H_2$ consumption peak below 0 °C in $H_2$-TPR(−70), because $H_2O$ formed as a product would re-adsorb on $H_2$ reduction sites and might prevent $H_2$ attack at these sites. Re-adsorption of $H_2O$ would affect the $H_2$ consumption profile, so we consider that two peaks at −15 and 20 °C indicate a reactive oxygen species. Therefore, we interpreted the $H_2$-TPR(−70) profile as having at least two kinds of oxygen on $Ag/ZrO_2$, a reactive oxygen species and another, less reactive oxygen species; these two types of oxygen species were assigned to $H_2$ consumption below room temperature and to the broad peak at 120 °C, respectively. The latter, less reactive oxygen species might have been $Ag_2O$, which was observed from XPS measurements to be present in the samples. Since the reduction of $ZrO_2$ was confirmed to proceed above 400 °C (not shown), we concluded that the reduction at 120 °C must not have corresponded to $ZrO_2$ reduction.

Assuming that the $H_2$ consumption in $H_2$-TPR(RT) corresponded solely to the oxygen contribution from $Ag_2O$, we calculated the amounts of reactive oxygen present in the catalyst system by subtracting the $H_2$ consumption in $H_2$-TPR(RT) from that in $H_2$-TPR(−70). We compared the amounts of these $H_2$ consumptions to the amounts of active oxygen species estimated from TPSR-CB, and we plotted both sets of values as a function Ag loading in Fig. 5. The $H_2$ consumption trends were quite different from those of the amount of active oxygen species. Therefore, the peaks in the

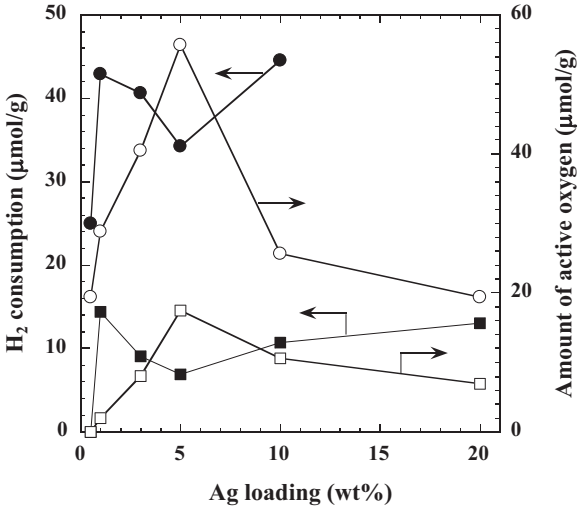


**Fig. 5.** Effect of Ag loading on $H_2$ consumption and amount of active oxygen observed in $H_2$-TPR. Symbols indicate $H_2$ consumption for reactive oxygen (●) and for oxygen from $Ag_2O$ (■), and the amount of the active oxygen species calculated from the peaks at low (○) and high temperatures (□) in Fig. 1.

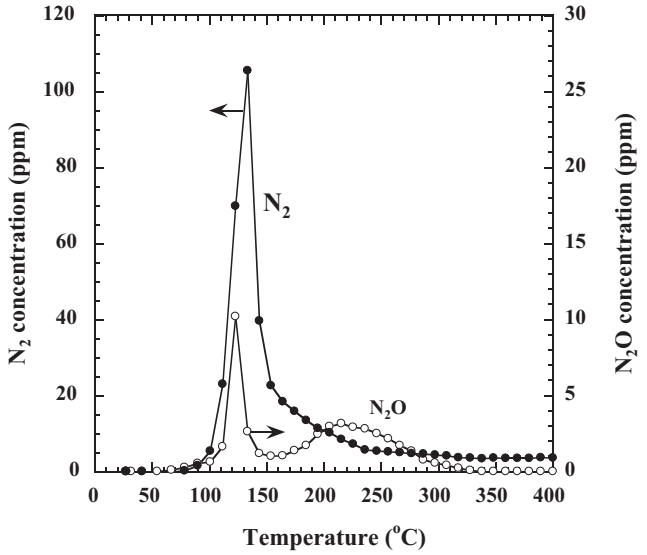


**Fig. 6.** $N_2$ (●) and $N_2O$ (○) formation profiles obtained from $NH_3$-TPR for 5 wt% $Ag/ZrO_2$.

$H_2$-TPR profiles did not directly reflect information on the two kinds of active oxygen species that were predicted from Fig. 1, and we concluded that the reactive oxygen species was not equivalent to the active oxygen species.

### 3.4. Characterization of active oxygen species by $NH_3$-TPR

We next used $NH_3$ as a reductant for temperature-programmed reduction. $NH_3$ is a weaker reductant than $H_2$, and therefore $NH_3$ is expected to analyze the reactive oxygen species in detail. The products of reduction by $NH_3$ are $N_2$ and $H_2O$, according to the following reaction equation:

$$3Ag_2O + 2NH_3 \rightarrow 6Ag + N_2 + 3H_2O.$$

Since $N_2$ re-adsorption hardly occurs, $N_2$ formation serves as an indicator of catalyst reduction. Moreover, if an oxygen species has a high oxidation capacity, it should form bonds with nitrogen to form $N_2O$ or NO. Thus, the $NH_3$-TPR products should indicate the oxidation capacity of the reactive oxygen species.

Fig. 6 shows an $NH_3$-TPR profile for 5 wt% $Ag/ZrO_2$. Prominent $N_2$ formation was observed at 135 °C. $N_2O$ formation was observed at 120 and 210 °C. The formation of $N_2O$ is evidence that certain oxygen species on $Ag/ZrO_2$ had strong oxidation capacity. We note that $N_2O$ decomposition did not occur at 135 °C over this catalyst, meaning that the $N_2$ observed here was formed directly from $NH_3$.

We compared $N_2$ and $N_2O$ formation profiles from $NH_3$-TPR for $Ag/ZrO_2$ with various Ag loadings (Fig. 7). Only one peak was observed for $N_2$ formation for all Ag loadings, and the temperature at which this peak occurred decreased slightly with increasing Ag loading. Two peaks corresponding to $N_2O$ formation were observed at 120 and 210 °C. Both peaks increased with increasing Ag loading up to 5 wt% and then decreased with increasing Ag loading above 5 wt%. The 0.5 wt% $Ag/ZrO_2$ catalyst exhibited no $N_2$ formation at 120 °C. The presence of one $N_2$ peak and two $N_2O$ peaks suggests that there are a few kinds of oxygen species present in the catalysts.

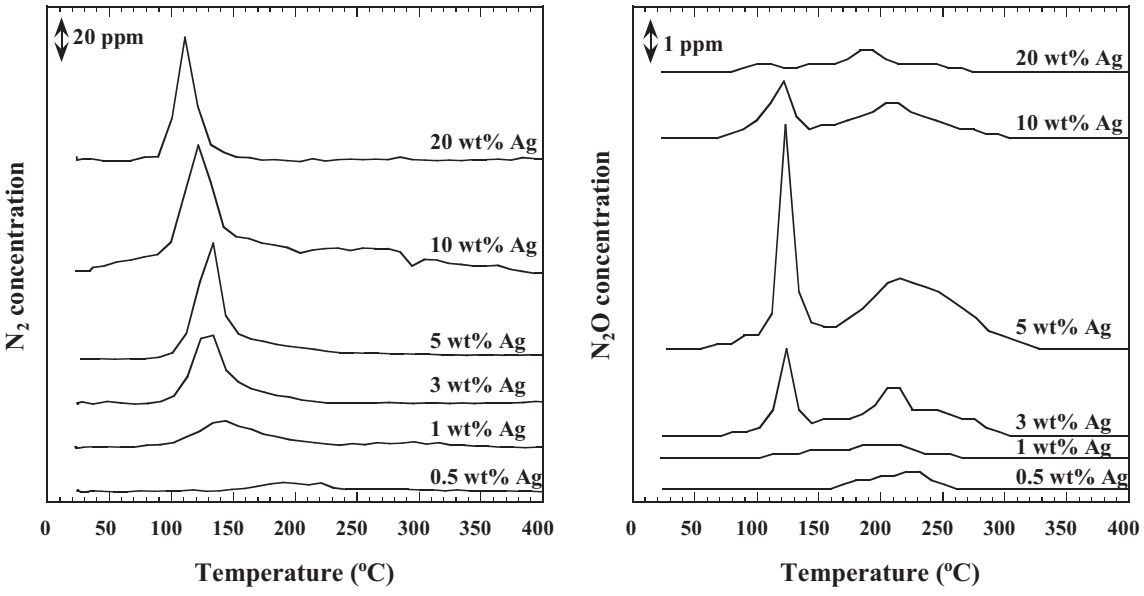


**Fig. 7.** Effect of Ag loading on the amounts of $N_2$ and $N_2O$ formed in $NH_3$-TPR and the amount of active oxygen calculated from TPSR-CB.

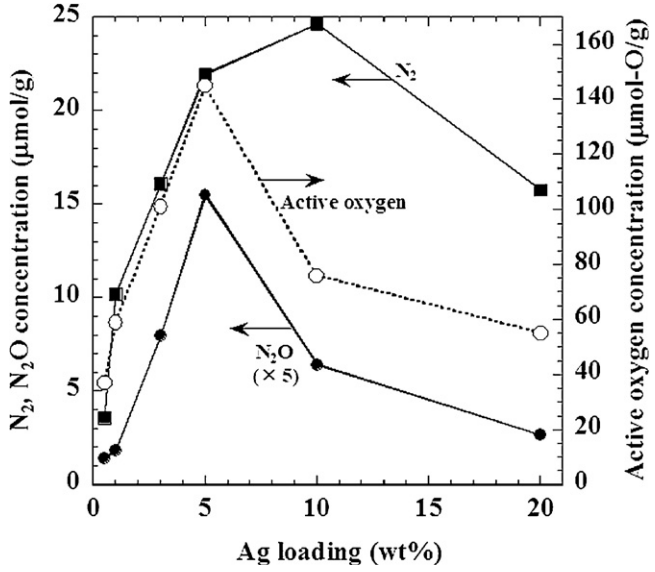


**Fig. 8.** Effect of Ag loading on the amounts of $N_2$ and $N_2O$ formation in $NH_3$-TPR and the amount of active oxygen species calculated from TPSR-CB results in Fig. 1. Symbols indicate the amount of $N_2$ (■) and $N_2O$ formation (●), and the amounts of active oxygen species (○).

Especially, the presence of two peaks for $N_2O$ formation in $NH_3$-TPR suggests that there are two kinds of oxygen species, which have a strong oxidation capacity.

Fig. 8 shows the effect of Ag loading on the amounts of $N_2$ and $N_2O$ formation in $NH_3$-TPR. $N_2$ formation increased with increasing Ag loading up to 10 wt% Ag. $N_2O$ formation also increased with increasing Ag loading up to 5 wt% Ag. The $N_2O$ formation trend was quite similar to that of the total amount of the active oxygen calculated from the profiles in Fig. 1, suggesting that the amount of $N_2O$ formation reflects the amount of active oxygen species present in the catalyst.

The amounts of $N_2O$ formation from both peaks in $NH_3$-TPR were compared to the amount of active oxygen species calculated from the low- and high-temperature peaks of TPSR-CB in Fig. 1, and the results of this comparison are shown in Fig. 9. Both

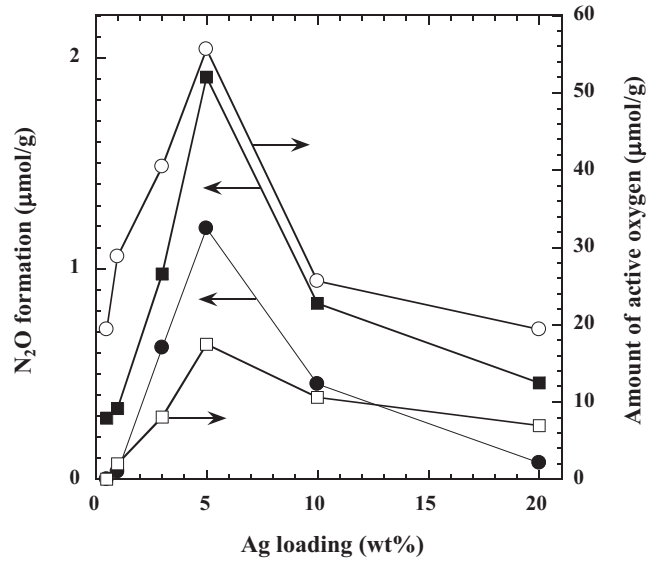


**Fig. 9.** Effect of Ag loading on the amount of $N_2O$ formation in $NH_3$-TPR and the amount of active oxygen. Symbols indicate the amount of $N_2O$ formation at low (●) and high temperatures (■), and the amounts of the active oxygen at low (○) and high temperatures (□).

the active oxygen species and $N_2O$ formation exhibit a clear peak at 5 wt% Ag loading. For the profiles of $N_2O$ formation, a low-temperature $N_2O$ peak (120 °C) was not observed for 0.5 wt% Ag loading, whereas the high-temperature peak (210 °C) was observed for all Ag loadings. The amount of $N_2O$ formation for the high-temperature peak was larger than that for the low-temperature peak. For the profile of the amount of the active oxygen species, the high-temperature peak (340–360 °C, open squares in Fig. 8) was not present at 0.5 wt% Ag loading, whereas the low-temperature peak (390–410 °C, open circles) was observed for all Ag loadings. The amount of the active oxygen species for the low-temperature peak was larger than that for the high-temperature peak. These results suggest that the low-temperature $N_2O$ peak was correlated with the high-temperature active oxygen species peak, and that the high-temperature $N_2O$ peak was correlated with the low-temperature active oxygen species peak. On the basis of these results, we concluded that $N_2O$ formation in $NH_3$-TPR can be used to quantitatively evaluate the amount of active oxygen species present on $Ag/ZrO_2$ for CB oxidation.

In contrast, the amount of oxygen consumed in the formation of $N_2O$ was not equivalent to the amount of active oxygen species estimated from these plots. According to the stoichiometric reaction for $N_2O$ formation, $4Ag_2O + 2NH_3 \rightarrow 8Ag + N_2O + 3H_2O$, the amount of consumed oxygen is 4 times larger than the amount of $N_2O$ formed. However, the amount of oxygen consumed for $N_2O$ formation was much lower than the amount of active oxygen species estimated from TPSR-CB (Fig. 1). One possible explanation for this large difference might be that the reaction of active oxygen species with $NH_3$ formed not only $N_2O$ but also $N_2$. We performed $NH_3$-TPR among $Ag/MgO$, $Ag/TiO_2$, and $Ag/Al_2O_3$ (not shown). We previously reported that Ag on $ZrO_2$ and MgO have mostly metallic state, and Ag on $TiO_2$ and $Al_2O_3$ is partially and mostly oxidized, respectively [23]. It is noted that $N_2O$ formation was observed only for $Ag/ZrO_2$. This result suggests that product distribution in $NH_3$-TPR does not depend on oxidation state of Ag.

The correlations between the low-temperature $N_2O$ peak and the high-temperature active oxygen species peak, and the high-temperature $N_2O$ peak and the low-temperature active oxygen species peak might be due to the difference of reaction mechanism of $NH_3$ and soot oxidation. $NH_3$ can react with all reactive oxygen species whereas soot might react with the specific oxygen species because cleavage of —C—C— bond in soot needs strong oxidation capacity. The high-temperature $N_2O$ peak in $NH_3$-TPR is assigned to the active oxygen species to break —C—C— bond. For $Ag/CeO_2$ catalyst, formation of the active oxygen for soot oxidation is involved in the interaction of Ag–$CeO_2$ [17,24]. The active oxygen species assigned to the high-temperature $N_2O$ peak might be in the neighbor of interface of Ag and $ZrO_2$. Once soot surface is activated, intermediates are formed on soot surface [25]. Since intermediates are more reactive than —C—C— bond, other oxygen species, which cannot react with —C—C— bond directly, migrate onto soot surface and react with intermediates at higher temperature than cleavage of —C—C— bond. The active oxygen species, which react with intermediates, might be adsorbed oxygen on Ag, and are indicated by the low-temperature $N_2O$ peak in $NH_3$-TPR. Studies to clarify the active oxygen species and its location on the catalyst are in progress.

## 4. Conclusions

Characterization of active oxygen species for soot oxidation over $Ag/ZrO_2$ were carried out. Our previous studies have shown that CB oxidation activity exhibits a sharp peak as a function of Ag loading, with a maximum at 5 wt% Ag loading. The temperature-programmed surface reaction of CB and preadsorbed oxygen suggested that there were two kinds of active oxygen

species present on the catalysts. However, because $O_2$-TPD profiles exhibited only one peak, the two active oxygen species were not distinguishable with this technique. Additionally, an $H_2$-TPR profile from room temperature exhibited only a small and broad $H_2$ consumption peak centered at 120 °C. In contrast, an $H_2$-TPR profile from −70 °C exhibited a large $H_2$ consumption peak below room temperature in addition to a small $H_2$ consumption peak around 120 °C. The observed $H_2$ consumption below room temperature suggested the presence of a reactive oxygen species. However, no relationship could be established between the amount of $H_2$ consumption and the amount of active oxygen species observed by TPSR-CB. We attempted $NH_3$-TPR with the expectation that $NH_3$, a weaker reductant than $H_2$, and its reduction products, $N_2$ and $N_2O$, could be used to distinguish the oxygen species on the basis of their different oxidation capacities. $NH_3$-TPR exhibited one $N_2$ formation peak and two $N_2O$ formation peaks. The presence of two $N_2O$ formation peaks suggests that at least two kinds of oxygen species were present. The effect of Ag loading on the total $N_2O$ formation was in good agreement with that on the amount of active oxygen observed from TPSR-CB. Moreover, the low-temperature $N_2O$ peak was correlated with the high-temperature active oxygen species peak in TPSR-CB, whereas the high-temperature $N_2O$ peak was correlated with the low-temperature active oxygen species peak. We concluded that $NH_3$-TPR is a powerful technique for quantitative characterization of the active oxygen species on $Ag/ZrO_2$ catalysts.

## Acknowledgement

This study was financially supported by the New Energy and Industrial Technology Development Organization (NEDO) of Japan.

## References

[1] V. Muzyka, S. Veimer, N. Schmidt, The Science of the Total Environment 217 (1998) 103–111.
[2] B.J. Cooper, H.J. Jung, J.E. Toss, US Patent No. 4902487 (1990).
[3] M. Machida, Y. Murata, K. Kishikawa, D. Zhang, K. Ikeue, Chemistry of Materials 20 (2008) 4489–4494.
[4] A. Setiabudi, J. Chen, G. Mul, M. Makkee, J.A. Moulijn, Applied Catalysis B 51 (2004) 9–19.
[5] K. Tikhomirov, O. Kröcher, M. Elsener, A. Wokaun, Applied Catalysis B 64 (2006) 72–78.
[6] K. Krishna, A. Bueno-López, M. Makkee, J.A. Moulijn, Applied Catalysis B 75 (2007) 189–200.
[7] T. Masui, K. Minami, K. Koyabu, N. Imanaka, Catalysis Today 117 (2006) 187–192.
[8] B.M. Reddy, P. Bharali, G. Thrimurthulu, P. Saikia, L. Katta, S.-E. Park, Catalysis Letters 123 (2008) 327–333.
[9] H. Shimokawa, H. Kusaba, H. Einaga, Y. Teraoka, Catalysis Today 139 (2008) 8–14.
[10] D. Fino, N. Russo, G. Saracco, V. Specchia, Journal of Catalysis 217 (2003) 367–375.
[11] I. Atribak, B. Azambre, A. Bueno López, A. García-García, Applied Catalysis B 92 (2009) 126–137.
[12] E. Aneggi, M. Boaro, C. Leitenburg, G. Dolcetti, A. Trovarell, Journal of Alloys and Compounds 408–412 (2006) 1096–1102.
[13] M. Issa, C. Petit, A. Brillard, J.F. Brilhac, Fuel 87 (2008) 740–750.
[14] D. Zhang, Y. Murata, K. Kishikawa, K. Ikeue, M. Machida, Journal of the Ceramic Society of Japan 116 (2008) 230–233.
[15] M.S. Gross, M.A. Ulla, C.A. Querini, Applied Catalysis A 360 (2009) 81–88.
[16] J. Liu, Z. Zhao, J. Wang, C. Xu, A. Duan, G. Jiang, Q. Yang, Applied Catalysis B 84 (2008) 185–195.
[17] K. Shimizu, H. Kawachi, A. Satsuma, Applied Catalysis B 96 (2010) 169–175.
[18] E. Aneggi, J. Llorca, C. de Leitenburg, G. Dolcetti, A. Trovarelli, Applied Catalysis B 91 (2009) 489–498.
[19] E. Saab, E. Abi-Aad, M.N. Bokova, E.A. Zhilinskaya, A. Aboukaïs, Carbon 45 (2007) 561–567.
[20] L.L. Murrell, R.T. Carlin, Journal of Catalysis 159 (1996) 479–490.
[21] T. Nanba, S. Masukawa, A. Abe, J. Uchisawa, A. Obuchi, in preparation.
[22] M.I. Zaki, M.A. Hasan, F.A. Al-Sagheer, L. Pasupulety, Colloids and Surfaces A 190 (2001) 261–274.
[23] T. Nanba, S. Masukawa, J. Uchisawa, A. Obuchi, Journal of Catalysis 259 (2008) 250–259.
[24] K. Yamazaki, T. Kayama, F. Dong, H. Shinjoh, Journal of Catalysis 282 (2011) 289–298.
[25] K. Krishna, A. Bueno-López, M. Makkee, J.A. Moulijn, Applied Catalysis B 75 (2007) 201–209.